

# Body Area Network channel model for Virtual-Reality applications

Carlos Aldana,<sup>1</sup> Connor Kennedy,<sup>2</sup> Morteza Mehrnoush,<sup>1</sup> Chunyu Hu,<sup>1</sup> and Andreas F. Molisch<sup>3</sup>

<sup>1</sup> Facebook, <sup>2</sup> Univ. Calif. Berkeley, <sup>3</sup> Univ. of Southern Calif.

Email: {caldana, mmehrnoch, chunyuhu}@fb.com, {cpk}@berkeley.edu, {molisch}@usc.edu

**Abstract**—Virtual reality (VR) setups often can be characterized as Body Area Networks (BANs) where one of the transceivers is mounted on the head of the user. In order to design and assess such systems, suitable channel models need to be established. This paper presents a novel model of the propagation channel covering both attenuation and delay dispersion for such BANs. The modeling approach separates the on-body propagation from the contributions of the environment, and is thus easy to generalize to other environments as well. The model is parameterized based on an existing measurement campaign, and can thus be directly used for BAN network simulations.

**Index Terms**—Body Area Network, Virtual Reality, path loss, delay dispersion, channel model

## I. INTRODUCTION

### A. Motivation

Virtual Reality (VR) and Augmented Reality (AR), often together called Extended Reality (XR), has the potential to revolutionize both the way we work, and the way we relax from work. While the headset is the visual centerpiece of an XR setup, it cannot operate by itself; rather it needs connection to both a processing unit (which is often mounted on the body or carried in a backpack, in order to provide sufficient mobility), and/or to sensors on the body. Communication between the headset and the peripheral units has to occur wirelessly, and in order to achieve high data rates and obtain precise localization information from the sensors (which is required for many XR applications), the connections should have large bandwidth. For this reason, ultra-wideband (UWB) communications are envisioned for XR applications, e.g., based on the IEEE 802.15.4z standard [1].

Due to interference from other systems in the frequency ranges between 3 and 6 GHz, as well as restrictions of the spectrum in various regions of the world current interest focuses on the frequencies between 6 and 8.5 GHz. Like for any wireless system, the design and assessment of such UWB-based VR-BANs requires knowledge of the propagation channel in which the system will operate.

### B. Existing work

Body Area Network (BAN) propagation channels have been investigated for several decades. Measurements have been mainly done for narrowband applications, in particular in the ISM bands. Obviously, all of these results cannot be applied

to UWB systems near 8 GHz, both due to the different center frequency and the smaller bandwidth of the measurements.

There have also been detailed investigations into UWB BAN channels. In particular, the 802.15.4a channel model [2] contains a model for UWB channels in an anechoic environment based on EM simulations. Measurement-based models have been based on measurements both inside an anechoic chamber and a lab or office environment, using a phantom [3], a single person [4]–[9], or groups of people [10], [10]–[14]. These models mostly cover the complete frequency range 3.1 – 10.6 GHz, and usually describe both the pathloss and delay dispersion. However, links are between different parts of the torso, or between limbs and torso. In this case, both the mounting of the antenna on the head is different, the orientation of an on-head antenna is different, and the shadowing by the human tissue near the antenna is different from the head-to-torso setup.

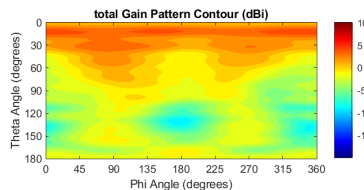
The number of UWB experimental investigations where at least one of the nodes is on the head is rather limited. Several papers investigate the propagation around the head [3], [15], [16]. Ref [17] measured from a single point on the torso to several points on the body so that body-to-head links are included, but there are only 3 of them, and measurements are only in an anechoic chamber. The closest work to our goals is [14], which performed and analyzed extensive BAN measurements between more than 100 different locations on the body that included multiple positions on the head. However, the model that is extracted from those measurements aims for a statistical description of the fading with the ensemble of the different measurement locations, mixing results between head-based and non-head-based links. This analysis thus does not provide a dependence of the pathloss on the specific placement of the nodes on the body, which is the aim of the current paper. A similar constraint holds for [10], which furthermore measures in a different frequency range (3 – 5 GHz), [18], which measures 5-7 GHz, and [11], which measures 3-10 GHz, but the latter two do not consider delay dispersion.

### C. Contribution of work

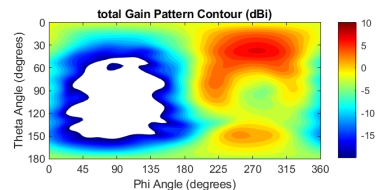
As the above literature survey has shown, there currently is no placement-dependent UWB model for propagation channels between head and torso. The current paper aims to fill this gap. In particular,



(a) Photo of used antenna for body mounting.



(b) Antenna pattern in free space



(c) Antenna pattern when antenna is mounted on a bottle of body-emulating dielectric fluid.

Fig. 1: Measurement antennas. From [19].

- we introduce a novel model structure for BANs that distinguishes on-body and off-body propagation, and can thus more flexibly combine precise measurements on the body with information about environmental reflections in a variety of environments;
- we present a parameterized channel model, describing both attenuation and delay dispersion, with simple closed-form fitting equations, based on an extensive measurement campaign [19].

## II. MEASUREMENT CAMPAIGN

The measurements that were used to parameterize the model in this paper were performed and documented in [19]. For the convenience of the reader, this section summarizes the measurement setup and environment.

### A. Measurement setup

The measurements were done with a Vector Network Analyzer (VNA), model SC5090 of Copper Mountain Technologies. The TX port was connected via an RF switch to two antennas and the RX port to four antennas. VNA, switch, and cables leading to the antennas were calibrated with an electronic calibration kit (model ACM2520). The motivation for the use of the VNA is the high accuracy of (calibrated) measurements with such a device. Like for all VNAs, wideband measurement of a transfer function can take a long time (order of 1 s) and thus does not allow determination of dynamics of the setup; but in the considered setup (phantom in a static environment), this is not of concern.

Measurements were performed over the bandwidth of 4.5 – 8.5 GHz, with frequency step width of 5 MHz, and IF bandwidth of 3 kHz. Switching between the different antenna elements was done through a Python script that controlled the RF switches. All transfer function measurements were repeated 20 times, which can be used to further improve SNR by noise averaging.

The employed antennas were AVX/Ethertronics Model 1005194 UWB antennas (see Fig. 1a), which are compact (dimensions 20.6 x 18.6 x 0.8 mm). The antenna is optimized for 6 – 8.5 GHz, but the actually used samples had acceptable VSWR (< 2) from 4.5 – 9 GHz. The two TX antennas were placed on the left and right side of the head. The RX antennas were placed on different locations of the torso. To ensure accurate and reproducible placement, velcro strips were used, and alignment markers indicated the exact location on



Fig. 2: Photo of human phantom "Popeye" with antennas and cabling. From [19].

the torso. To maintain constant spacing between phantom and antenna, 4 mm thick foam spacers were used. The antenna pattern measured in a near-field chamber can be seen from Fig. 1b that it is reasonably omni-directional. However, large dielectric objects distort the pattern. Since the phantom itself was too large to be placed in the near-field chamber, its effect was emulated by placing the antenna on a bottle filled with dielectric liquid with similar properties as the phantom. The distorted antenna pattern is shown in Fig. 1c.

### B. Environment

Popeye is a brand of phantoms manufactured by SPEAG AG, and certified for over-the-air testing, emulating the dielectric and loss properties of a typical human. The specific model used in the measurement campaign emulates the body type of a male in good physical shape (used by the Canadian army). Since stability of the phantom when standing is a problem, only head, arms, and torso were used, and placed on a stack of styrofoam bricks that were placed on a plastic cart, so as to minimize reflections from the mounting, see Fig. 3.

Antennas were placed on the phantom on a vertical line on the left side of the torso (directly under the TX antenna on the left side of the head), with distance from that TX antenna of 30, 40, 50, and 60 cm. Furthermore, antennas were placed on the circumference of the body, at angles  $n \times 30^\circ$ ,  $n = 0, 1, 2, \dots, 11$ , at a vertical distance of 50 cm from the TX. Cables for both the TX and RX antennas were placed and fixed in place carefully to minimize impacting the antenna patterns and the propagation paths from TXs to RXs, see Fig. 2.



Fig. 3: Photo of human phantom "Popeye" in the "Office with Desk" environment. From [19].

The measurements were performed in three environments: (i) an anechoic chamber, (ii) an empty office, where the phantom was placed in the center of the office, and (iii) an office with furniture, including a standing desk and monitor, with the phantom placed in front of the desk. The office had dimensions  $3.5 \times 3.9$  m; in the office with the desk, the phantom was directly in front of the desk, with a distance of about 1.25 m to the wall behind the desk. Further measurements were done in an outdoor environment; results are not shown here for space reasons but show similar trends, for details see [20].

### III. DATA PROCESSING AND SAMPLE RESULTS

#### A. Data processing

For the evaluation of impulse responses and pathloss, the antennas are considered as part of the propagation channel, since a de-embedding of the antenna characteristics is very difficult in particular when placing antennas on different parts of the body. The output of the measurements is a 5-dimensional matrix  $H_{i,j,k,m,e}$ , where  $i$  and  $j$  index the RX and TX antenna position, respectively,  $k$  is the subcarrier  $k = 0, \dots, 800$ ,  $m$  indexes the repetition of the measurement  $m = 0, \dots, 19$ , and  $e$  the environment (1 is the anechoic chamber, 2 the empty office, and 3 the office with desk).

The first processing step is the (coherent) averaging over the 20 measurement repetitions. We then for each combination  $i, j, e$  obtain an 801 element vector that is extended with nulls in the frequency domain to 8192 entries before inverse fast Fourier transform (IFFT), providing an oversampled version of the impulse response  $h(\tau)$ , and the power delay profile  $P(\tau) = |h(t, \tau)|^2$ . The impulse response is both delay gated (components beyond 6ns delay in the anechoic chamber, and 120ns in the office are disregarded), and a noise threshold is implemented (samples are set to 0 if they are below a threshold that is 6dB above the noise floor). The samples of the power delay profile (PDP) are then binned, i.e., all samples falling within a 2ns bin width are added up to provide a tapped delay line model with a regular spacing of the taps. Note that this approach leads to an effective bandwidth of 500 MHz, and thus does not fully exploit the potential of the 4 GHz measurement bandwidth. This was partly motivated by the fact that typical UWB applications use 500 MHz bandwidth

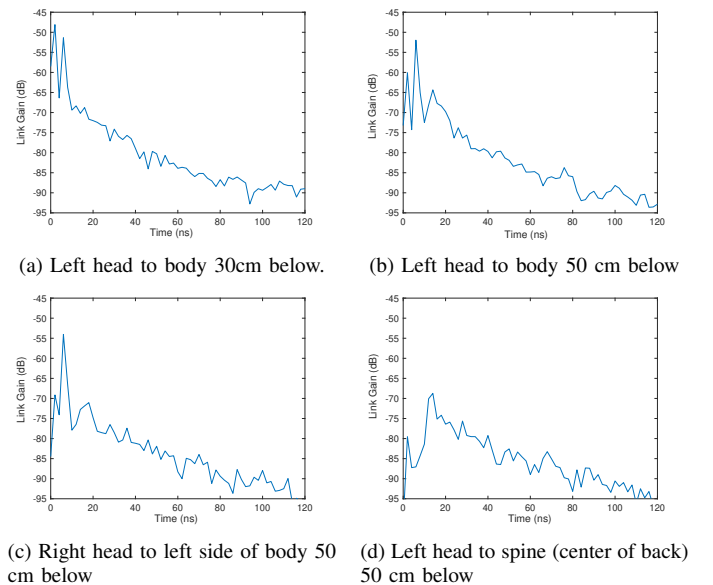


Fig. 4: Squared magnitude of impulse response for channel from head to body in office environment with desk.

(the minimum that is considered UWB) [21]. Exploiting wider bandwidth, including high-resolution extraction of the delays of the multipath components (MPCs) is the topic of ongoing and future work. The total received power, from which the pathloss is computed, is obtained by summing up the power of the samples in the delay domain.<sup>1</sup>

#### B. Sample results

Figure 4 shows several sample results of the PDP in an office environment with a desk (for clarity, only the delay range  $[0, \dots, 120\text{ns}]$  is shown). In Fig. 4a, the TX is directly over the RX, and only 30 cm away. This leads to a strong peak in the first PDP at  $2\text{ns}$  delay, with a second peak at  $6\text{ ns}$  that corresponds to the reflection from the monitor. There is furthermore an exponentially decaying component starting at around  $12\text{ns}$ , which corresponds to the MPCs reflected by the environment. Fig. 4b shows the PDP when the RX is 50 cm below the TX antenna. We observe that the screen-reflected components have remained essentially unchanged, while the direct component has decreased by more than 10 dB, i.e., much more than expected from Friis' law. This is because this antenna is on the belly of the phantom, which is shadowed off by the chest (this effect would not occur in a person with a protruding belly). This effect is even stronger if the RX antenna is mounted on the right side of the head; we conjecture that this is due to the fact that the Rx antenna has a lateral offset from the Tx on the right side of the head, which compounds the misalignment of the main lobes of the antennas. Finally, if the RX is on the back of the phantom, the direct component (diffracting around the body and/or

<sup>1</sup>While the resulting path gain is not exactly identical to the path gain computed in the frequency domain in the  $6.25 - 6.75$  GHz frequency range, we verified that the difference between these quantities is less than 0.5 dB.

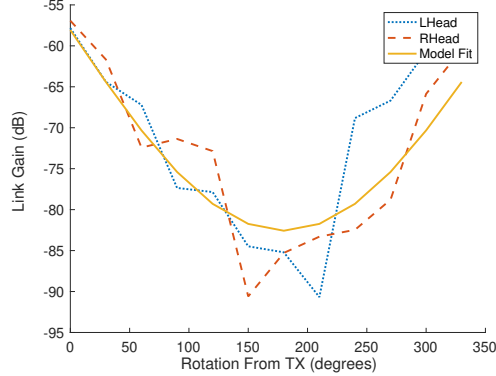


Fig. 5: Link gain from the left and right side of the head to the different positions on the circumference on the body, and sinusoidal fit.

propagating as surface wave) is very strongly attenuated, but now the screen-reflected MPC is completely absent. Rather, MPCs propagating via back- and sidewall reflections provide the dominant contributions.

#### IV. MODEL

To model the channel in the considered environments, we propose to split the MPCs into contributions of on-body propagation, screen reflection (if they occur), and room reverberations. This is of obvious usefulness in the modeling of the PDPs as discussed above, but can also be applied for the computation of the received power. One key advantage of this approach is that the on-body propagation, which is always present, but most difficult to model, can be measured once, e.g., in an anechoic chamber, and later combined with the room reverberations from a variety of environments, such as office, residential, industrial hall, etc. To validate this idea, we compared the on-body contributions in the 3 measured environments, and found good agreement (within the limits of reproducibility of antenna placement) between them.

##### A. Pathloss model for on-body propagation

We first analyze the dependence of the path gain on the position of the RX antenna along the circumference of the body. Fig. 5 shows the measured result for both the situation when the TX antenna is on the left and the right side of the head. In the coordinate system of the measurements, 0 degree is defined in the middle of the chest (sternum), and 180 degree at the spine. The 30 degree point is approximately aligned with the left side of the body where the vertical line of measurement points is located, while 330 degree is aligned with the right side of the head. A good fit for the dependence of the link gain on the angle is

$$G_{c,\text{dB}}(\phi) = \alpha_c + \beta_c \sin(\phi/2) + S_c \quad (1)$$

where  $\phi$  is the *difference in angle* between the location of the TX and the observation point,  $S_c$  are shadowing variations with standard deviation  $\sigma_c$ , and  $\alpha_c$ ,  $\beta_c$ , and  $\sigma_c$  are parameters to be extracted from the measurements.

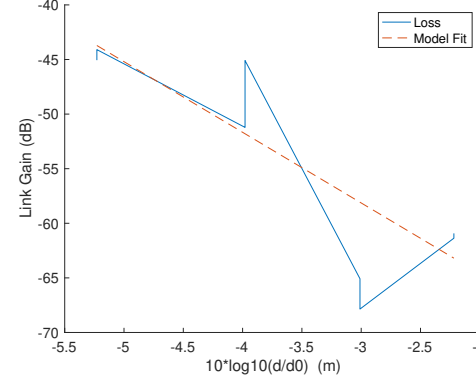


Fig. 6: Link gain from the left side and right side (adjusted for circumference displacement) of the head to the different positions on the front of the body, and linear fit.

For the dependence of the link gain on the vertical distance, we use the traditional power law

$$G_{v,\text{dB}}(d) = \alpha_v + 10\beta_v \log(d/d_0) + S_v \quad (2)$$

where  $d_0$  is the reference distance which we arbitrarily set to 1m, and the other parameters have a similar interpretation as for the circumference model.

A consistent model will then ensure that  $\alpha_c = G_{v,\text{dB}}(d)$ . In other words, link gain can be obtained, for any location and angular offset as

$$G_{c,\text{dB}}(\phi) = \alpha_v + 10\beta_v \log(d/d_0) + \beta_c \sin(\phi/2) + S \quad (3)$$

where  $S$  describes the total variations around the model fit. The parameters of this model are summarized in Table I. We firstly find a large intercept value  $\alpha_v$ , which is caused by the fact that our chosen reference distance is *larger* than the distances at which we measure (this of course has no impact on the results). We secondly observe a strong dependence of the path gain on the distance, with a slope of more than 6, compared to a free-space slope of 2. This strong distance dependence is caused partly by the fact that at farther distances, intervening body parts shadow off the free-space connections. Another contribution might arise from the fact that the antenna is placed tangential to the body shape at the mounting location, so that different RX locations have the RX antenna with different angles with respect to the vertical line, and thus different antenna gains.

Finally, note that at this time, it is only a conjecture that the link gain indeed follows this model; in particular it is possible (and even likely) that  $\beta_c$  depends on the vertical distance  $d$ . However, since no measurements are available at the time of this writing that would allow to verify this hypothesis and quantify such a dependence, we retain the simple model (3).

##### B. Path gain for environmental contributions

The contributions of the screen reflection and the environmental reflections can be described by similar functions, though the resulting parameters are significantly different. In particular, the dependence of the path gain on the vertical

scenario	on-body	screen	environment
$\alpha_v$	-77.4	-51.9	-61.1
$\beta_v$	-6.5	-1.1	-0.25
$\beta_c$	-27.3	-21.4	-4.5
$\sigma_v$	5.2	4.7	0.73
$\sigma_c$	6.2	8.1	1.7

TABLE I: Parameters of the path gain model for on-body contribution, screen contribution, and environment contribution.

param	$\tau_2$ [ns]	$\gamma_1$ [dB/tap]	$\gamma_2$ [dB/tap]	$a_1/a_2$ [dB]	Dev. PDP [dB]
$\alpha_v$	29.7	-1.42	-0.31	9.33	—
$\beta_v$	—	—	—	-0.52	—
$\beta_c$	25.0	0.65	0.058	3.9	—
$\sigma_v$	9.1	0.28	0.036	1.8	1.68
$\sigma_c$	14.5	0.26	0.044	2.39	1.70

TABLE II: Parameters for delay dispersion model in empty office.

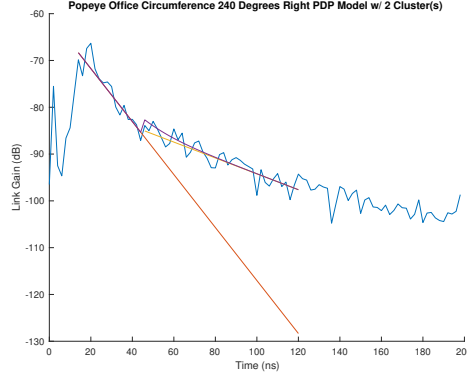


Fig. 7: PDP in office environment, from right side of head to on-body position 240 deg circumference. Also shown are two-cluster fit to environmental contribution, and the sum of those two clusters.

distance is *much* lower, since no shadowing by body parts impacts these components, and the influence of the variations of the antenna patterns is also greatly reduced.

#### C. Delay model

We now turn to the delay dispersion, i.e., modeling of the PDP. In most of the literature, a single-exponential decay has been assumed for BANs both in anechoic chambers and in indoor environments. Already the sample PDPs of Fig. 4 show this to be a bad fit. Rather, the following model should be used

$$PDP(\tau) = a_{\text{on-body}} \delta(\tau - \tau_{\text{LOS}}) + a_{\text{screen}} \delta(\tau - \tau_{\text{screen}}) + \sum_{n=1}^{N_{\text{cluster}}} a_n \exp [(\tau - \tau_n) \gamma_n] I(\tau \geq \tau_n) \quad (4)$$

where  $I(x)$  is the indicator function, which is 1 if the argument is true, and 0 otherwise. With our settings, the fine structure (shape) of the on-body contribution could not be resolved, and the  $\tau_{\text{LOS}}$  is always in the bin centered at 2 ns; similarly  $\tau_{\text{screen}} = 6$  ns and  $\tau_1 = 12$  ns. We furthermore found for all measured scenarios  $N_{\text{cluster}} = 2$  to provide a good fit. It was not possible, however, to provide a clear association between the parameters of the two-cluster environmental reflections and the geometry of the room; rather the best-fit parameters show considerable variations as a function of the location of the antennas on the body. Figure 7 shows a typical fit. Note that the exponential cluster fit is not perfect, so that there are variations around these fitting values in each delay bin, which also have to be modeled.

This model contains a number of parameters that need to be fitted. Notably, the on-body and screen-reflected components

param	$\tau_2$ [ns]	$\gamma_1$ [dB/tap]	$\gamma_2$ [dB/tap]	$a_1/a_2$ [dB]	Dev. PDP [dB]
$\alpha_v$	53.6	-0.97	-0.24	13.3	—
$\beta_v$	—	—	—	-0.68	—
$\beta_c$	-7.2	0.10	-0.11	-4.76	—
$\sigma_v$	15.5	0.37	0.066	1.57	1.61
$\sigma_c$	17.5	0.41	0.21	3.41	1.71

TABLE III: Parameters for delay dispersion model in office with desk.

are already parameterized through the path gain model, since we observe only a single MPC, at a fixed location (within the resolution of the system). Rather, the parameters that need to be described are (i) the start of the second cluster  $\tau_2$ , (ii) the slopes of the time decay of first and second cluster,  $\gamma_1$  and  $\gamma_2$ , (iii) the power ratio between the peak of the first and second cluster,  $a_1/a_2$ , and (iv) the deviation of the PDP in each delay tap from the modeled (exponential) decay.

Notably, for many of those parameters we could not observe a dependence on the vertical distance. This may be partly due to the relatively small number of measurement points, so that the confidence intervals of fits of linear distance dependence include both positive and negative slopes. Furthermore, we observed that when modeling the cdf of the parameters, it was usually not Gaussian but rather uniform. This is aligned with physics since, e.g., cluster slopes  $> 0$  (i.e., clusters that become stronger with increasing delay) do not make sense. Summarizing, we use the following models:

- For  $\tau_2$ ,  $\gamma_1$ ,  $\gamma_2$ : distance-independent  $\alpha_v + S_v$  along the vertical; and  $\alpha_v + \beta_c \sin(\phi/2) + S_c$  along the circumference, i.e., consistency of vertical and horizontal model is again enforced. The deviations of all parameter values from the mean are uniform, *not* normal.
- For deviation of the PDP in each tap from the exponential model: deviations from the mean are distributed lognormal.
- For ratio of first to second peak  $a_1/a_2$  in dB: model in Eq. (3), with deviations that are uniformly distributed.

Note that possible correlations between different parameters are neglected, since the amount of available data does not allow a reliable extraction. The results of the fits can be found in Tables II and III.

#### D. Simulation procedure

Based on the above-extracted parameters and models we can now describe the steps to simulate channels that agree

with the measurement results

- 1) Determine the path gain of on-body: use Eq. (3) with the parameters of Table I and distance and angle according to location of the nodes on the body. Add stochastic variations (modeled as lognormal) according to  $\sigma_V$  and  $\sigma_C$  in Table I.
- 2) Determine path gain of the contribution from the screen reflection, and the environment contributions, in a similar manner,
- 3) For PDP, the on-body contribution is a delta pulse at delay tap 2ns. The power of this tap follows from the above-computed path gain.
- 4) The screen reflection contribution is a delta pulse at delay tap 6ns; again the power follows from the path gain of this component.
- 5) The starting point of cluster 1 is 12ns; starting point of second cluster is chosen from the circumference-dependent delay distribution. Delay does not depend deterministically on vertical distance, but an extra variance is added.
- 6) Pick the decay time constants for 1st and 2nd cluster at random, from the model with the parameters of Table II or III, depending on the environment.
- 7) Pick ratio of first to second peak at random, from the model with the parameters of Table II or III, depending on the environment.
- 8) Compute the power of sum of the first and second cluster in interval [12, ...120ns], and normalize so that the previously selected power of environmental reflections is reproduced.
- 9) The PDP at each delay tap is deterministically computed (from the two exponentials), together with a normally distributed (on a dB scale) statistical variation around it according to the parameters of Tables II and III.

## V. CONCLUSIONS

This paper has presented a detailed statistical model for the head-to-torso BAN propagation channel. Separating out the contributions of on-body and environmental propagation, we established a flexible and fully parameterized (based on existing measurements) model that provides path gain and power delay profiles as a function of the mounting position of the antennas on head and torso. The model can thus serve as a basis for design and evaluation of VR systems. Future steps will include (i) a larger number of antennas on the torso to verify the decomposition of path gain into vertical and circumferential terms, (ii) modeling with larger bandwidths, and (iii) verification of the measurements with human test subjects; such tests are currently under way and will be reported in [20].

## REFERENCES

- [1] P. Sedlacek, M. Slanina, and P. Masek, "An overview of the ieee 802.15.4z standard its comparison and to the existing uwb standards," in *2019 29th International Conference Radioelektronika (RADIOELEKTRONIKA)*. IEEE, 2019, pp. 1–6.
- [2] A. F. Molisch, D. Cassioli, C.-C. Chong, S. Emami, A. Fort, B. Kannan, J. Karedal, J. Kunisch, H. G. Schantz, K. Siwiak *et al.*, "A comprehensive standardized model for ultrawideband propagation channels," *IEEE Transactions on Antennas and Propagation*, vol. 54, no. 11, pp. 3151–3166, 2006.
- [3] T. Zasowski, G. Meyer, F. Althaus, and A. Wittneben, "Uwb signal propagation at the human head," *IEEE Transactions on Microwave Theory and Techniques*, vol. 54, no. 4, pp. 1836–1845, 2006.
- [4] A. Fort, J. Ryckaert, C. Dessel, P. De Doncker, P. Wambacq, and L. Van Biesen, "Ultra-wideband channel model for communication around the human body," *IEEE Journal on Selected Areas in Communications*, vol. 24, no. 4, pp. 927–933, 2006.
- [5] A. Fort, C. Dessel, P. De Doncker, P. Wambacq, and L. Van Biesen, "An ultra-wideband body area propagation channel model-from statistics to implementation," *IEEE Transactions on Microwave Theory and Techniques*, vol. 54, no. 4, pp. 1820–1826, 2006.
- [6] A. Fort, F. Keshmiri, G. R. Crusats, C. Craeye, and C. Oestges, "A body area propagation model derived from fundamental principles: Analytical analysis and comparison with measurements," *IEEE Transactions on Antennas and Propagation*, vol. 58, no. 2, pp. 503–514, 2009.
- [7] T. Kobayashi, "Recent progress of ultra wideband radio propagation studies for body area network," in *2009 2nd International Symposium on Applied Sciences in Biomedical and Communication Technologies*. IEEE, 2009, pp. 1–6.
- [8] T. Zasowski, F. Althaus, M. Stager, A. Wittneben, and G. Troster, "Uwb for noninvasive wireless body area networks: Channel measurements and results," in *IEEE Conference on Ultra Wideband Systems and Technologies*, 2003. IEEE, 2003, pp. 285–289.
- [9] Q. H. Abbasi, M. U. Rehman, S. Liaquat, and A. Alomainy, "Multiple input multiple output radio channel characterisation for ultra wideband body centric wireless communication," in *2013 IEEE International RF and Microwave Conference (RFM)*. IEEE, 2013, pp. 238–242.
- [10] X. Chen, X. Lu, D. Jin, L. Su, and L. Zeng, "Channel modeling of uwb-based wireless body area networks," in *2011 IEEE international conference on communications (ICC)*. IEEE, 2011, pp. 1–5.
- [11] M. M. Khan, M. A. Rahman, A. Alomainy, and C. Parini, "Ultra wideband on-body radio propagation channels study for different real human test subjects with various sizes and shapes," in *2013 2nd International Conference on Advances in Electrical Engineering (ICAEE)*. IEEE, 2013, pp. 323–328.
- [12] S. Sangodoyin and A. F. Molisch, "Impact of body mass index on ultrawideband mimo ban channels?measurements and statistical model," *IEEE Transactions on Wireless Communications*, vol. 17, no. 9, pp. 6067–6081, 2018.
- [13] F. Di Franco, C. Tachtatzis, B. Graham, M. Bykowski, D. C. Tracey, N. F. Timmons, and J. Morrison, "The effect of body shape and gender on wireless body area network on-body channels," in *IEEE Middle East Conference on Antennas and Propagation (MECAP 2010)*. IEEE, 2010, pp. 1–3.
- [14] R. Di Bari, Q. H. Abbasi, A. Alomainy, and Y. Hao, "An advanced uwb channel model for body-centric wireless networks," *progress in electromagnetics research*, vol. 136, pp. 79–99, 2013.
- [15] D. Bresnahan and Y. Li, "Investigation of creeping wave propagation around the human head at ism frequencies," *IEEE Antennas and Wireless Propagation Letters*, vol. 16, pp. 2767–2770, 2017.
- [16] R. Chandra and A. J. Johansson, "A link loss model for the on-body propagation channel for binaural hearing aids," *IEEE Transactions on Antennas and Propagation*, vol. 61, no. 12, pp. 6180–6190, 2013.
- [17] T. Kumpuniemi, T. Tuovinen, M. Hämäläinen, K. Y. Yazdandoost, R. Vuohoniemi, and J. Iinatti, "Measurement-based on-body path loss modelling for uwb wbanc communications," in *2013 7th International Symposium on Medical Information and Communication Technology (ISMICHT)*. IEEE, 2013, pp. 233–237.
- [18] V. Sipal, D. Gaetano, P. McEvoy, and M. J. Ammann, "Impact of hub location on the performance of wireless body area networks for fitness applications," *IEEE Antennas and Wireless Propagation Letters*, vol. 14, pp. 1522–1525, 2014.
- [19] K.T., "Measurement for body channel modeling," report to Facebook, Tech. Rep., 2021.
- [20] T. B. Determined, "A channel model for body area networks in indoor environments for virtual-reality applications," *IEEE Transactions on Wireless Communications*, p. to be submitted, 2022.
- [21] "First report and order 02-48," Federal Communications Commission, Tech. Rep., 2002.